Acta Pharmaceutica Sinica B 2020;10(8):1563−1575

Chinese Pharmaceutical Association
Institute of Materia Medica, Chinese Academy of Medical Sciences

Acta Pharmaceutica Sinica B

www.elsevier.com/locate/apsb
www.sciencedirect.com

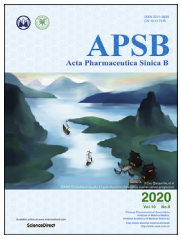

ORIGINAL ARTICLE

Bone marrow mesenchymal stem cells-derived exosomes for penetrating and targeted chemotherapy of pancreatic cancer

Yu Zhou[a], Wenxi Zhou[b], Xinli Chen[b], Qingbing Wang[a], Chao Li[b], Qinjun Chen[b], Yu Zhang[b], Yifei Lu[b], Xiaoyi Ding[a,*], Chen Jiang[b,*]

[a]*Department of Interventional Radiology, Ruijin Hospital, Shanghai Jiao Tong University, School of Medicine, Shanghai 200025, China*
[b]*Key Laboratory of Smart Drug Delivery, Ministry of Education, State Key Laboratory of Medical Neurobiology, Department of Pharmaceutics, School of Pharmacy, Fudan University, Shanghai 200032, China*

Received 24 August 2019; received in revised form 1 October 2019; accepted 1 November 2019

KEY WORDS

Pancreatic cancer;
Exosomes;
Drug delivery;
Penetration;
Target therapy

Abstract Pancreatic ductal adenocarcinoma (PDAC) is one of the most intractable malignancy, with an only 6% 5-year relative survival rate. The dismal therapeutic effect is attributed to the chemotherapy resistance and unique pathophysiology with abundant inflammatory cytokines and abnormal hyperplasia of extracellular matrix (ECM). Based on the theory that bone marrow mesenchymal stem cells (BM-MSCs) can influence the tumorous microenvironment and malignant growth of PDAC, we employed exosomes (Exos) derived from BM-MSCs as PDAC-homing vehicles to surpass the restrictions of pathological ECM and increase the accumulation of therapeutics in tumor site. To overcome chemoresistance of PDAC, paclitaxel (PTX) and gemcitabine monophosphate (GEMP)—an intermediate product of gemcitabine metabolism—were loaded in/on the purified Exos. In this work, the Exo delivery platform showed superiorities in homing and penetrating abilities, which were performed on tumor spheroids and PDAC orthotopic models. Meanwhile, the favorable anti-tumor efficacy *in vivo* and *in vitro*, plus relatively mild systemic toxicity, was found. Loading GEMP and PTX, benefitting from the naturally PDAC selectivity, the Exo platform we constructed performs combined functions on excellent penetrating, anti-matrix and overcoming chemoresistance (Scheme 1). Worth expectantly, the Exo platform may provide a prospective approach for targeted therapies of PDAC.

*Corresponding authors. Tel./fax.: +86 21 51980079 (Chen Jiang); +86 21 34186589 (Xiaoyi Ding).
E-mail addresses: dxy10456@rjh.com.cn (Xiaoyi Ding), jiangchen@shmu.edu.cn (Chen Jiang).

Peer review under the responsibility of Chinese Pharmaceutical Association and Institute of Materia Medica, Chinese Academy of Medical Sciences.

https://doi.org/10.1016/j.apsb.2019.11.013

1. Introduction

Pancreatic ductal adenocarcinoma (PDAC) continues to be a devastating malignancy with 1-year and 5-year relative survival rate close to 27% and 6% respectively. Furthermore, the incidence rate is increasing by 1.3% every year[1]. Besides lower rates of early diagnosis and surgical resection[2], unsatisfactory effectiveness of gemcitabine-based chemotherapy regimens also accounts for the dilemma of PDAC treatment[3]. On one hand, abnormally abundant extracellular matrix (ECM) in tumor environment leading to the pathophysiological barrier, extremely deficient tumor related neovascularization, both compromise the penetration of cytotoxic chemotherapeutics and concentrating in the tumor tissue[4]. On the other hand, chemotherapy resistance greatly reduces the sensitivity of chemotherapeutics, which was resulted from the declined activity of gemcitabine (GEM) metabolic limited enzymes and insufficient transformation of GEM phosphorylated products[5]. Therefore, the improvement of the chemotherapeutic effect requires not only overcoming the compact barrier of ECM for the preferential accumulation of anticancer agents, but also enriching medicative GEM phosphorylated products.

Nanotechnology-based drug delivery system offers alternative strategies for treating this intractable disease[6], especially for overcoming the pathophysiological barrier of PDAC[7]. Therapeutic avenue that depleting acellular stromal components, including collagen and hyaluronan, was utilized to remove the restrictions of matrix and increase penetration and homogenous distribution of nanomedicines, such as PH20, Hedgehog-pathway inhibitors and oncolytic virus loaded nanocarriers[8–10]. However, accompanied with the collapse of ECM, growth space and spread pathway were provided for the tumor parenchymal cells, leading to tumor proliferation and increase of metastasis probability[11]. Alternatively, reduction of solid stress follows targeting tumor mesenchymal cells can normalize the intratumoral fluid pressure and enhance the blood perfusion, also is regarded as a practicable solution. For instance, nab-paclitaxel (nab-PTX, Abraxane, a commercialized target drug) plus GEM regimen prolong the median overall survival, theoretically benefitting from the active targeting ability of albumin to SPARC that is rich in the tumoral mesenchyma[12]. Insufficiently, interrupting the crosstalk between tumor cells and mesenchymal cells may enhance the invasiveness of residual tumor cells, as well as metastasis probability[13]. Therefore, endeavors should be urgently demanded to develop novel systems with capabilities of efficient targeting and penetrating, meanwhile, circumventing the tumor ECM barrier.

Exosomes (Exos), which have shown superiorities in the field of drug delivery, are defined as a subtype of extracellular vesicles categorized by diameter of 40–120 nm and released by enormous variety of cells[14]. The recognized function of Exos as vesicles of intercellular communication has been further developed in the delivery of therapeutics, such as chemicals, genes, and even proteins, by diverse methods[15,16]. As bio-vectors derived from cells, Exos show low immunogenicity *in vivo*, also scalability or reproducibility in the process of collection[17,18]. Inherited signatures from parental cells, Exos can target specific region naturally, named homing selectivity[19]. Additionally, chemically modified or gene-engineered Exos designed to deliver chemotherapeutics in the implanted subcutaneous tumor models[20–22] show that editable or modified Exos still maintain themselves' original properties and can effectively enhance the tumor targeting.

Based on the osculating relationship between bone marrow mesenchymal stem cells (BM-MSCs) and PDAC, as well as the theory of "bone marrow–pancreatic cancer axis"[23,24], Exos derived from BM-MSCs may provide promising options for targeting PDAC site effectively. Meanwhile, some functional membrane proteins will amplify the homing effect[25,26]. What's more, Exos may perform excellent penetrability in region that stroma highly expressed, in which process dominated by crucial membrane proteins[27,28]. Due to the different pathway in penetrating mechanism, Exos derived from BM-MSCs may reach the deep sites of PDAC directly, and such characteristic makes this type of Exos different from the traditional strategies. Consequently, Exos nano-formulation perform therapeutic effect accumulationally in the tumor cellular components surrounded by the matrix, subsequently improves the effectiveness and pertinence, if appropriate anti-tumor therapeutics would be delivered by the Exos.

To achieve an expected poisonousness in the chemoresistance PDAC model, various elaborate formulations loaded GEM were designed, aiming at improving the uptake of GEM by diverse styles of internalization instead of original transportation *via* human equilibrative nucleotide transporter 1 (hENT1)[29]. There are still some deficiencies of nanocarriers including liposomes, polymeric nanoparticles, polymer micelles and inorganic nanoparticles, for instance, short half-life, low bioavailability, instability or organic accumulation[7,29,30]. Besides, the crucial problem that insufficient GEM phosphorylated products, which arise out of declining activity of GEM metabolic limited enzymes, still remains unsolved[5]. Direct delivery of gemcitabine monophosphate (GEMP)—an intermediate product of GEM metabolism—provides advisable option that can sort above problem out. However, neither passive diffusion nor active transportation can mediate the uptake of GEMP into cells, indicating that GEMP should be modified or supported by nanocarriers before it can be transported into cytoplasm[31].

Inspired by the above work, we attempted to employ BM-MSCs-derived Exos loading chemotherapeutics to target pancreatic cancer, aiming at penetrating and accumulating efficiently, as well as overcoming chemoresistance simultaneously (Scheme 1). Exos were isolated and purified from BM-MSCs supernatant, and loaded with GEMP and PTX *via* different approaches to form a co-delivery platform. The capability of targeting and penetrating in an orthotopic PDAC model was validated, and then the anti-tumor potency was investigated both *in vivo* and *in vitro*. Meanwhile, systematic safety was appraised after intravenous administration of the formulation. In summary, the BM-MSCs-derived Exos nanomedicine could provide a promising approach for targeted therapies of PDAC.

2. Materials and methods

2.1. Isolation of BM-MSCs derived Exos

For the culture of BM-MSCs (ScienCell, San Diego, CA, USA), we firstly need an Exo-depleted fetal bovine serum (FBS; Gibco, Carlsbad, CA, USA). Twenty mL FBS were filtrated with 0.22 μm syringe filters (Meck-Millipore, Billerica, MA, USA), subsequently centrifuged overnight at 150,000×*g*, 4 °C, once again filtrated with 0.1 μm syringe filters for the preparation of cultural medium.

Replacing BM-MSCs medium (ScienCell) with corresponding medium containing 10% Exo-depleted FBS when cells adhered to the wall, then continuously cultured for 48 h. Supernatant were collected and following centrifuged at 800×*g*, 4 °C for 10 min to

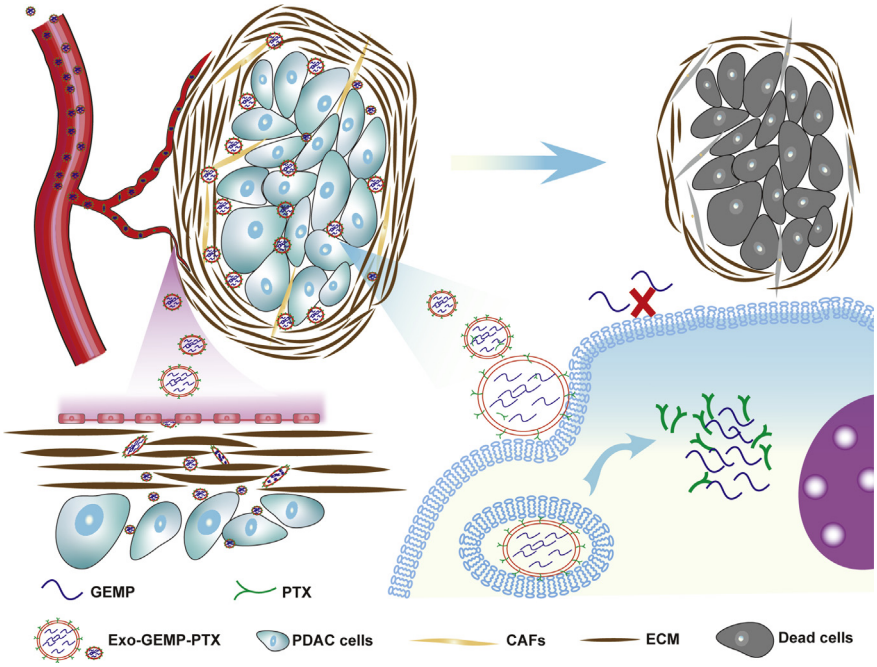

Scheme 1 The exosomal co-delivery platform performs combined functions on excellent stromal penetrability, anti-matrix and overcoming chemoresistance.

remove the dead cells. Centrifugation at 2500×*g* for 15 min was applied to remove the debris and at 15,000×*g* for 30 min to remove the large vesicles. The fluids were filtrated with 0.22 μm syringe filters, then condensed the medium to 20 mL by ultrafiltration units (MWCO 100 kDa, Meck-Millipore), following centrifuged at 150,000×*g*, 4 °C for 2 h. Discarded the supernatant and dispersed the pallets with 500 μL PBS 7.4. Then the gradient medium was made as shown in Fig. 1A with OptiPrep™ (Sigma−Aldrich, Billerica, MA, USA), which is a 60% (*w*/*v*) solution of iodixanol in water. Five hundred μL pallets were loaded on top of the gradient medium, and then centrifuged at 120,000×*g*, 4 °C for 16 h. With 1 mL pipettes, samples were collected respectively in 12 tubes from top to bottom, and numbered them orderly. A refractometer was applied to assess the density of every phase. According to the density of Exos between 1.13 and 1.19 g/mL, fluids in tube of Nos. 6 and 7 were collected and diluted to 20 mL with PBS 7.4, subsequently washed twice at 150,000×*g* (4 °C, 2 h). Pallets on the bottom were dispersed with 500 μL fresh PBS 7.4 and stored at −80 °C.

2.2. *Characterizations*

For detecting the concentration and hydrated diameters of Exos, 100 μL Exos solution were diluted to 1 mL with fresh PBS 7.4, analyzed by nanoparticles tracking analysis (NTA; NanoSight NS300, Malvern Panalytical, Malvern, UK). CD9, CD63, TSG101 and Flotllin-1 were verified by Western blotting as the biomarkers of Exos. To observe the morphology of Exos, appropriately diluted samples were loaded on a carbon film coated copper grid, dried in the air, then stained by 1.0% phosphotungstic acid solution for 2 min. Washed on drop of fresh PBS for twice and dried naturally, observed the samples under TEM (Tecnai G2, FEI, Hillsboro, OR, USA).

2.3. *Probe labeling and loading GEMP and PTX into Exos*

Bodipy (λ_{Ex} = 650, λ_{Em} = 665, Thermo Fisher, Waltham, MA, USA) dissolved in DMSO with a concentration of 1 mg/mL was used to label and track the Exos. 5 μL Bodipy solution was added in 500 μL Exos, disposed in 37 °C water bath, 1 h for recovery after labeled by sonicating for 3 min with 35 W power. The unbonded probe was removed using an exosome spin columns (MW 3000, Invitrogen, New York, NY, USA) according to the procedure. The same protocol was applied in labeling Exos with IR780 (λ_{Ex} = 750, λ_{Em} = 800) for tracking the Exos *in vivo*. For labeling HSA with bodipy, 1 eq. HSA and 1.2 eq. Bodipy were added in PBS 8.0, and continuously reacted for 24 h, then dialyzed in ddH_2O for 24 h. Products were freeze-dried and re-dissolved in PBS 7.4 for the next experiment.

To load GEMP, a reversible electroporation method was applied as described in previous study[32]. Exos (10^9) dispersed in 400 μL OptiPrep™-based electroporation buffer mixed with 2.0 mg GEMP were processed with parameters set as 400 V, 125 μF and ∞Ω (Gene Pulser X Cell Electroporation System, Bio-Rad, Hercules, CA, USA). Immediately transferred the mixture onto ice for recovery 1 h, following diluted to 2 mL with PBS 7.4 preparing for the process of loading PTX. Two mg of PTX dissolved in 200 μL DMSO was slowly added into previous mixture drop by drop, a sonic protocol[33] was performed to load PTX, subsequently incubated at 37 °C, 1 h to allow recovery for Exos membrane. Unbounded drugs were removed by centrifuged twice at 10,000 rpm (Allegra X-12, Beckman Coulter, Brea, CA, USA) and ultra-filtrated three times with PBS 7.4 at 3900×*g* until the volume was concentrated to 500 μL.

The amount of GEMP and PTX loaded into Exos were measured by HPLC method. Five hundred μL Exo-GEMP-PTX solution was freeze-dried and dissolved in 600 μL methanol. Then

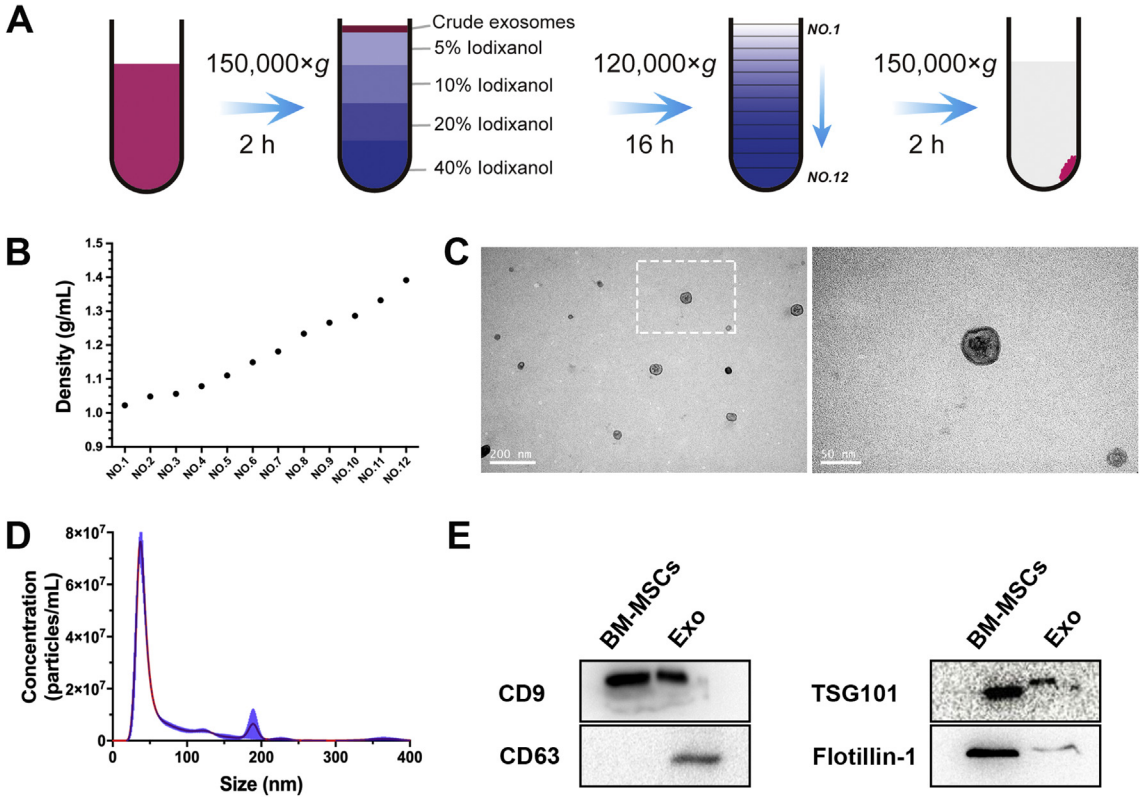

Figure 1 Isolation and characteristics of Exos. (A) Schematic protocol of isolation and purification of Exos. (B) Density distribution of each tube. (C) TEM images of Exo, scale bars represent 200 and 50 nm respectively. (D) NTA results of diameter and concentration, samples were diluted 10 times with PBS 7.4. (E) Biomarkers certified by Western blotting.

20 μL samples were injected into HPLC system (Agilent 1220, Agilent, Santa Clara, CA, USA), analyzed using a C18 column (Sigma−Aldrich) at a flow rate of 1.0 mL/min at 26 °C. To analyze the concentration of GEMP, mobile phase contained 40 mmol/L ammonium acetate (97%) and methanol (3%) was applied, additionally, concentration of PTX were measured with a mobile phase of ACN/H_2O (55/45, *v*/*v*). Absorbance was measured at 268 nm to monitor the elution of GEMP, and at 227 nm for PTX.

2.4. *Investigation of internalization and degradation in MiaPaca-2 cells*

MiaPaca-2 cells were seeded in 6-well plates at a density of 1.5×10^5 cells per well for the investigation of internalization of Exos. After cultured for 24 h, cells were respectively pre-incubated for 0.5 h with different pathway inhibitor (1 μg/mL filipin, 1 μg/mL colchicine and 0.3 μg/mL PhAsO) in 4 °C, and then washed with Hanks' buffer for three times. Equal bodipy-labeled Exos were added and further cultured in incubation for 6 h. For the study of intracellular location, 3.0×10^3 cells were seeded in a confocal dish and continued cultured for 24 h. Exchanged the medium with DMEM containing appropriate Exo-Bodipy, following incubated at 37 °C with 5% CO_2 for 6 h, then removed the supernatant and slightly washed three times. Cellular nucleus was stained with 1.0 μg/mL DAPI solution for 10 min and acid organelles were stained with Lysotracker Green DND-26 (Thermo Fisher) in 37 °C for 30 min.

2.5. *Preparation of 3D tumor spheroids and confocal imaging*

Mixed medium containing 2% agarose (*w*/*v*) in base DMEM were heated by microwave for 5 cycles (5 s/cycle), following swelled in oil-bath at 80 °C for 30−40 min, finally sterilized. MiaPaca-2 cells (4.0×10^3/well) were dropped on the concave surface of condensational mixed medium, which was prepared by pipetting 150 μL per well sterile mixed medium onto a 48-well plate and naturally concreted. Continuously incubated at 37 °C with 5% CO_2 for 5−7 days without exchange of medium, tumor spheroids were observed and transferred to confocal dish for the next incubation with formulations.

To evaluate efficiency of penetration, different formulations including nomadic bodipy, HSA-Bodipy and Exo-Bodipy were adjusted to equal fluorescence intensity previously, then incubated with spheroids respectively ($n = 3$) at 37 °C with 5% CO_2 for 6 h. Upon slightly rinsed with PBS for three times, the spheroids were subjected to confocal microscope (LSM710, Carl Zeiss, Oberkochen, Germany) and imaged employing z-stack model.

2.6. *Preparation of the orthotopic PDAC model*

MiaPaca-2 cells were harvested by 0.25% trypsin (Gibco) and resuspended in appropriate Hanks' buffer. Nude mice were anesthetized by intraperitoneal injection of 250 μL 0.6% pentobarbital sodium solution, then fixed and sterilized. Incision about 0.8 cm located on the left mid-abdomen was made. The subcutaneous tissue and muscles were opened orderly to expose spleen,

followed with slight pulling out spleen with cotton swabs to expose pancreas. Cells (8.0×10^5) in 80 μL Hanks' buffer were subcapsular injected into one pancreas slowly, sutured the muscles and incision carefully after recovered organs. Sterilized again and kept animals warming until revived. After 12−14 days, the volume of tumors was measured by intraperitoneal injection of D-luciferin potassium solution (3 mg D-luciferin potassium in 100 μL PBS 7.4) and manifestation using *in vivo* imaging system (IVIS; Caliper, Perkin Elmer, Waltham, MA, USA). The animal experiments were carried out in strict accordance with guidelines evaluated and approved by Fudan University Institutional Animal Care and Use Committee (IACUC) and Ethics Committee with the accreditation number as 2016-03-MHYY-WQB-01.

2.7. Tracking and biodistribution of exosomes in vivo

In vivo imaging study of Exos distribution was carried out on orthotopic PDAC models ($n = 3$). Nude mice were intravenously injected with nomadic bodipy and Exo-Bodipy at equivalent bodipy dose of 0.8 mg/kg. The mice were anesthetized and visualized *via* near-infrared signal at $\lambda_{Ex/Em}$ 650/665 nm respectively at 1, 4, 8, 12, 24 and 48 h post injection. Meanwhile, at 48 h, specific location of tumors was visualized *via* luminescence signal by intraperitoneal injection of D-luciferin potassium solution. Upon 48 h, tumor-bearing mice were anesthetized and perfused with saline and 4% paraformaldehyde orderly, following whole tumor tissues and major organs were harvested. Fluorescence intensity of tumors and organs at 650/665 nm were measured employing IVIS system.

To investigate the penetrating capability of Exos, frozen slides and immunofluorescent staining were carried out. After fixed in 4% paraformaldehyde for 20 h, tumors were dehydrated with 10%, 20% and 30% sucrose solution for 24 h gradually. Embedded with OCT medium at −20 °C, samples were cut into slides at 10 μm thickness. Combining with anti-collagen I and anti-α-SMA monoclonal antibodies (Abcam, Cambridge, UK), targets were visualized by binding with AF488 conjugated secondary antibodies. After stained with DAPI, samples were subjected to confocal imaging analysis.

2.8. In vitro anti-tumor efficacy study

Anti-tumor efficacy was evaluated by MTT assay, cells apoptosis and cycle inhibition. For MTT assay, MiaPaca-2 cells were seeded in 96-well plates at a density of 5.0×10^3 cells per well. After cultured for 20 h, cells were treated with different formulations at various concentration and cultured for 48 h in an incubation ($n = 4$). Subsequently, removed the drug contained medium, carefully rinsed tumor cells with Hanks' buffer for three times, then 100 μL MTT solution (0.5 mg/mL) per well was added. After continued cultured for 4 h at 37 °C, the solution was removed and 150 μL DMSO was added to dissolve the formazan crystal. Cell viability was measured by microplate spectrophotometer (Epoch2, BioTek, Winooski, VT, USA) and IC_{50} was calculated by GraphPad Prism 8.0 (La Jolla, CA, USA).

For apoptosis assay, MiaPaca-2 cells were seeded in 24-well plates at a density of 1.0×10^4 cells per well and cultured for 24 h at 37 °C, 5% CO_2. Then cells were treated with different formulations for 15 h ($n = 3$), 1 μmol/L GEM was added in GEM and Exo-GEM group, correspondingly, in GEM+nab-PTX group, 1 μmol/L GEM and 1.11 μmol/L nab-PTX (correspond as 0.11 μmol/L PTX) were added. In the Exo-GEMP-PTX group, addition dose was calculated according as 1 μmol/L GEMP. As a control, Exos were added at a concentration of carriers in 1 μmol/L GEMP. Furtherly, tumor cells were stained with an apoptosis kit as direction, then subjected to detection by flow cytometry (CytoFLEX S, Beckman Coulter, Brea, CA, USA).

To investigate the characteristics of drug efficacy, cycle inhibition assay was performed on MiaPaca-2 cells by a Cell-cycle Analysis kit 1.0×10^5 cells per well tumor cells were seeded in 6-well plates and culture for 20 h. Concentration of adding drugs were same with apoptosis assay, then cells were treated for 10 h, following removed the drug contained medium ($n = 3$). After digested by 0.25% trypsin, cells were fixed in 75% ethanol overnight. Carefully washed with PBS 7.4 twice, tumor cells were stained using the kit as protocol, finally measured by flow cytometry (FACSCanto II, BD, Franklin Lakes, NJ, USA).

As for detection of dose of GEMP in cellular plasm, 1.5×10^5 cells per well tumor cells were seeded in 6-well plates and culture for 24 h. The same concentration of drug in apoptosis and cycle inhibition assay was added to incubate cells. Upon 8 h post addition, the incubation was terminated and the sample was digested with 0.25% trypsin. The cells were disposed by sonic for 5 min at 35 W, followed by repeated freeze-thawing. The samples were freeze dried and the protein concentration was measured respectively. Fluids containing 100 μg proteins were freeze dried again, and then disposed as HPLC analysis protocol.

2.9. In vivo anti-tumor efficacy

Forty tumor-bearing mice were randomized into five groups ($n = 8$) and intravenously injected with Exos, GEM, Exo-GEM, GEM+nab-PTX and Exo-GEMP-PTX in every 3 days at a dose corresponded with 10 mg/kg GEM and 10 mg/kg GEMP, added up to 6 doses. Meanwhile, mice body weight was recorded every three days until the 27th day. To study the efficacy in vision of tissue level, animals ($n = 3$) were sacrificed after 6 doses on the 27th day, followed with a harvest of tumor samples, paraffin sections and frozen slides were prepared for H&E staining and immunofluorescent staining. Also, major organs (heart, liver, spleen, lung, kidney and intestine) incised from treated mice were stained by H&E staining assay. The volume of tumors was measured by detection of bioluminescence every five days ($n = 5$) until the 25th day. Continuously feed the mice until naturally dead to obtain the survival curves.

For immunofluorescent staining, tumors excised from the pancreatic models on the 27th day were fixed in 4% paraformaldehyde for 24 h and dehydrated with 10%, 20% and 30% sucrose solution for 24 h gradually. The tumor tissues were then frozen in OCT embedding medium at −20 °C and sectioned at 10 μm thickness. The as-prepared samples were then stained with TUNEL and Ki67 before being observed by fluorescence microscope (Leica, Wetzlar, Solms, Germany). The frozen slides were also immunofluorescence stained with anti-collagen I and anti-α-SMA monoclonal antibodies, then subjected to confocal microscopy analysis (Carl Zeiss LSM710, Wetzlar, Solms, Germany).

2.10. Statistical analysis

Analysis was performed using ImageJ 1.8.0 (Bethesda, MD, USA), GraphPad Prism 8.0 and SPSS 22.0 (Arkmont, NY, USA), and the results were presented as means ± SD. Statistical comparisons among two groups were performed by unpaired student *t*-test, and comparisons between multiple groups were assessed by

one-way ANOVA. Statistical significance was defined as $^{***}P < 0.01$, $^{**}P < 0.05$.

3. Results and discussions

3.1. Synthesis and characteristics of GEMP

A mixed solution contained 34 mL $(MeO)_3PO$ and 23 mL $POCl_3$ was continuously and rapidly stirred on ice, meanwhile, 1 g gemcitabine compound was added into the above solution slowly, and allowed to react for 2 h below 5 °C. Deionized ice water was then added into the solution, which was then extracted by 100 mL $CHCl_3$ twice. The aqueous layer was adjusted to pH 6.5 with strong aqua ammonia below 30 °C. $CHCl_3$ was used to extract again, and the aqueous layer was lyophilized. The solid was collected and resolved into 100 mL methanol, stirred for 1 h, filtered, and followed by evaporation. Silica column chromatography was applied in elution with isopropanol, aqua ammonia and water (7:2:1), subsequently disposed with iron-exchange resin to give 437.82 mg final product with a yield of 43.78%. The product was characterized with ^{1}H NMR and ^{13}C NMR spectrum after dissolved the product in D_2O, suggesting the successful preparation of GEMP (Supporting Information Fig. S1).

3.2. Isolation and purification of Exos

High purity is required in the application of Exos as nano-vector for drug delivery[17], or else the impurities would influence drug loading or physiological processes *in vivo*. Aiming at that, we performed a classic density gradient centrifugation protocol (Fig. 1A) to isolate and purify Exos. Following continuously centrifuged for 16 h at 120,000×*g*, the whole fluid was divided into 12 equal parts (1 mL per tube). Meanwhile, a refractometer was applied to measure the density of each tube (Fig. 1B). The density of Nos. 6 and 7 was measured to be 1.149 and 1.181 g/mL, respectively, according the density distribution of Exos should be between 1.13 and 1.19 g/mL[34]. Exos were naturally fixed and contrasted with phosphotungstic acid prior to transmission electron microscope (TEM) have a bowl shape appearance (Fig. 1C). More importantly, low background without proteins or other impurities contaminated suggests the high purity of Exos. Average diameter of Exos is 75.5 ± 1.4 nm (mean ± SD) analyzed by nanoparticles tracking analysis (NTA) system. The concentration was detected to be (1.57 ± 0.09) × 10^{10} particles/mL (Fig. 1D). Biomarkers including CD9, CD63, TSG101 and Flotillin-1 were certified positively by Western blotting (Fig. 1E) among characteristics of Exos.

3.3. Internalization and degradation mechanisms in MiaPaca-2 cells

Efficient cellular uptake is prerequisite for effective drug delivery. As to Exos, different sources and subtype of integrins on the membrane may lead to diverse outcome of uptake[15,35,36]. There has been no study to elucidate the uptake mechanism in detail, especially for BM-MSCs-derived Exos in pancreatic cancer cells. To investigate this process, MiaPaca-2 cells were pretreated with different inhibiting conditions known to interfere with different pathways following incubated with Exos labeled by bodipy for 6 h. As shown in Fig. 2A and Supporting Information Fig. S2, in the group predisposed with PhAsO, red fluorescence expression changed inapparently compared to the normal group (37 °C), indicating that clathrin-dependent pathway mainly influences internalization of Exos barely. Significant red signals decrease in the other groups was found, illustrating the sufficiently that Exos internalized in MiaPaca-2 cells dependent on energy, mediated by clathrin-independent endocytosis and macropinocytosis.

We further investigated the degradation of Exos. Exos (red) were found colocalized endo-cellularly with acid organelles (green, Fig. 2B), such as lysosomes and late endosomes, denoting that Exos were ultimate degraded in these organelles after cellular uptake. As depicted in previous studies, contents in Exos were released in late endosomes, meanwhile an acidic pH could enhance this process[36], thus chemotherapeutics loaded in Exos would be released endo-cellular effectively.

3.4. Penetration in 3D tumor spheroids

Different from other cancer target therapies, there is immensely abnormal expression of ECM around PDAC parenchymal cells, which can construct a compact physiologic barrier for nanoparticles penetrating into, leading to dissatisfactory therapeutic endings[37]. Tumor spheroids are reported as versatile 3D models for evaluating penetration and efficacy *in vitro*, sharing similarities with morphology and biology microenvironment in solid tumors[38]. To investigate the capability of penetrating deeply utilizing Exos platform, we constructed a 3D PDAC spheroid model to mimic the pathologic barrier in PDAC. Meanwhile, human serum albumin (HSA)-labeled by bodipy (HSA-Bodipy) was designed as a positive control, due to its recognized performance in clinical application so far.

In this experiment, tumor spheroids were incubated with nomadic bodipy, HSA-Bodipy and Exo-Bodipy respectively for 6 h, subsequently observed at 16.58 μm fixed intervals. The diameters of the tumor spheroids in three groups were 324.84 ± 21.70 (bodipy group), 328.13 ± 32.08 (HSA-Bodipy group) and 344.38 ± 22.57 μm (Exo-Bodipy group), respectively. As shown in Fig. 2C, red signals expressed barely in the interior hypo-nutritional region, both in the bodipy and HSA-Bodipy groups. However, in the Exo-Bodipy group, red hyperintensities emerged in the hypo-nutritional region, at the bottom (layers 1−6) and top right (layers 1−3). Visualized on 2.5D models of layer 6, which represented the central layer of spheroids, we also observed Exos could penetrate through the hyper-nutritional region containing plenty of viable cells compared with bodipy and HSA-Bodipy (Fig. 2D). To evaluate the penetrating efficiency quantitatively, red fluorescence expression in hyper-nutritional and hypo-nutritional region were concluded by ImageJ 1.8.0, following divided. Contrasted to bodipy (25.72 ± 3.03%) and HSA-Bodipy (29.87 ± 3.90%) in the ratio of penetration, there are significant superiority for the Exo-Bodipy group (39.88 ± 5.11%, $^{***}P < 0.01$, $^{**}P < 0.05$, Fig. 2E).

Exos are depicted as vesicle-shape, phospholipid bilayer, where versatile biomarkers like CD47, annexin-V and so on were over-expressed[25,39]. Tetraspanins, a 4-transmembrane protein family[40], form complexes located in tetraspanin-enriched membrane domains, which facilitate vesicular fusion and/or fission[41]. Clearly, members of tetraspanins family like peripherin/RDS were shown to alter the membrane curvature[42], resulting in deformation of Exos what may benefit its striding over the compact intercellular connections. Evidences also show that a tetraspanin-like protein encoded by gene *PLS1* in the fungal pathogen *Magnaporthe grisea* is required for rice leaf penetration[28]. Besides, in the

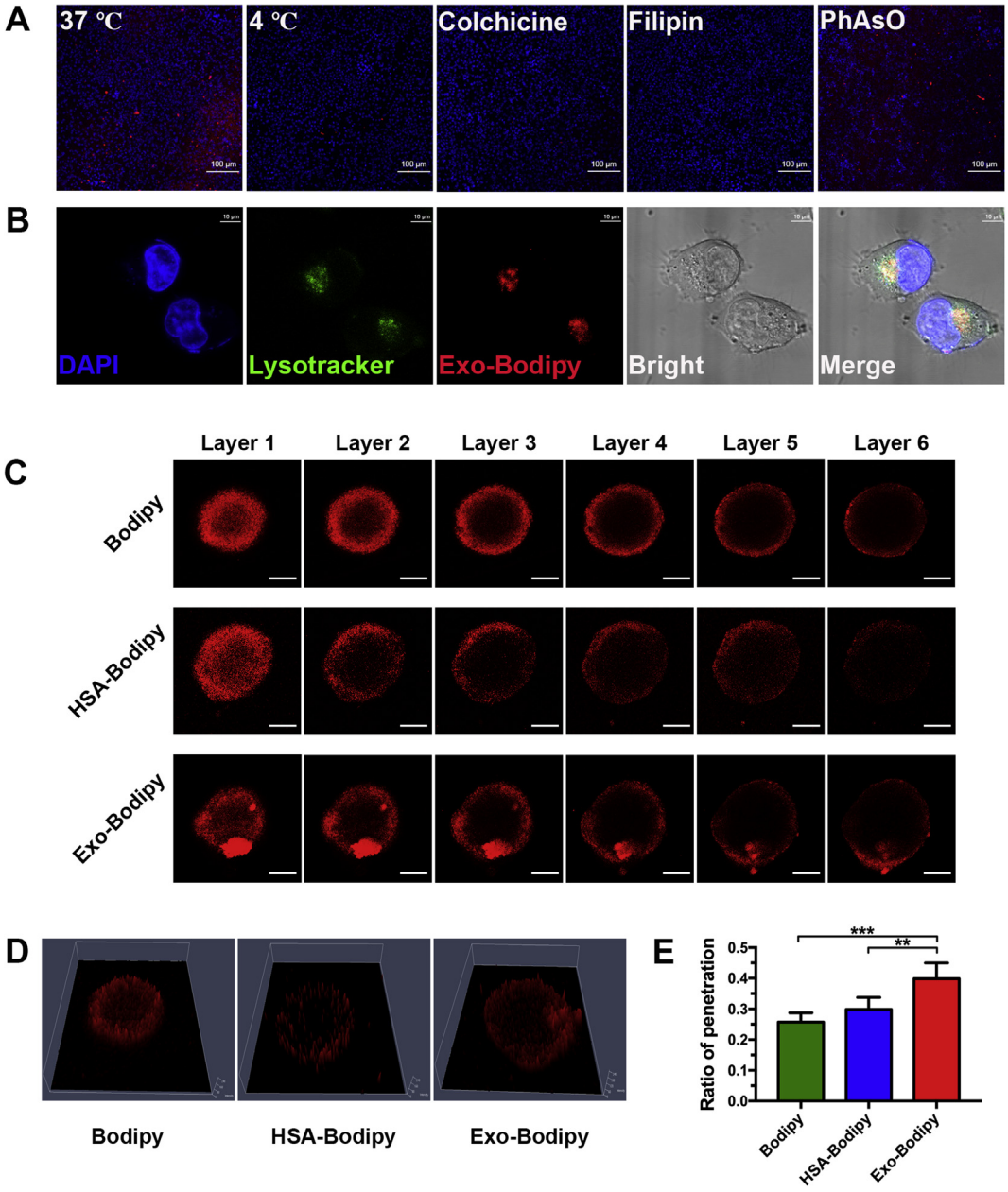

Figure 2 Uptake and internalization mechanisms for BM-MSCs derived Exos in MiaPaca-2 cells, penetration in 3D tumor spheroids with 6.0 h of incubation. (A) Investigating internalization, amplified 100×, scale bars represent 100 μm. (B) Degradative location of Exos in MiaPaca-2 cells, acid organelles stained by Lysotracker (green) and Exos labeled with bodipy (red), amplified ×630, oil lens, scale bars represent 10 μm. (C) Probe (red) distribution in the 3D tumor spheroids, layers 1−6 represent top to central layer, interval 16.58 μm, amplified 200×, scale bars represent 100 μm. (D) 2.5D model of layer 6. (E) Ratio of penetration, $^{**}P < 0.05$, $^{***}P < 0.01$.

process of penetration, the tetraspanin complexes enable Exos to target cell selective capability[35] also contributes to the preferable penetration.

3.5. *Accumulation and penetration in PDAC orthotopic model*

It has not been studied particularly that if Exos derived from BM-MSCs could home to PDAC or not, despite Exos from other resources have shown their superiorities in target therapies of various cancers. Certainly, targeting capacity of material plays an indispensable role in achieving preferable therapeutic efficacy. To verify our hypothesis that BM-MSCs derived Exos can home to pancreatic cancer efficiently *in vivo*, luciferase stable-transfected MiaPaca-2 cell lines were implanted in nude mice pancreas to prepare an orthotopic PDAC model. The biodistribution was investigated following intravenously injected IR780 labeled Exos (Exo-IR780) and nomadic IR780, by observation at predesignated time points (1, 4, 8, 12, 24, and 48 h, Fig. 3A). Within 4 h, a majority of nomadic IR780 accumulated rapidly in liver, but in the Exo-IR780 group, relative fewer in liver, indicating that Exos has a relatively prolonged circulation time. At the point of 12 h, Exos were found to start the accumulation in the tumor, while most of

the nomadic IR780 had been metabolized from liver and kidney. From 24 to 48 h, Exo-IR780 displayed prominent and permanent accumulation in the tumor regions contrasted with nomadic probe, which had been excreted completely. Simultaneously, luciferin was intraperitoneally injected to manifested specific tumor location at 48 h (Fig. 3A, right), definitely confirming that Exos could home to PDAC efficiently, especially red fluorescence signal distribution was consistent with tumor bioluminescence. Distribution in major organs (heart, liver, spleen, lung, kidney and intestine) and whole tumor tissue was detected (Fig. 3B), and quantified (Fig. 3C), showing that Exos demonstrated significant homing capability.

To further investigate the improved penetration of Exos *in vivo*, aforementioned process was repeated with Exo-Bodipy, where collagen I was evaluated as ECM, α-SMA represented fibroblasts in tumor mesenchyma. As shown in Fig. 3D, Exos distributed homogenously in tumor, even though collagen I expressed densely in large quantities. Such phenomenon was also observed in Fig. 3E, it indicates that Exos could penetrate into tumor efficiently and target either parenchymal cells or mesenchymal cells.

Now that experimental results have confirmed our hypothesis, and it definitely demonstrates that BM-MSCs derived Exos would be an effective delivery material of targeting PDAC. In the expectant process, multiple factors enabled Exos functions of homing to parenchyma and striding the ECM barrier: 1) passive target benefited from EPR effect based on the appropriate nanoparticle size, though its limited and inconspicuous role in targeting PDAC[43]; 2) chemotaxis, because of abundant inflammatory cytokines released in the proinflammatory setting of PDAC, and immigration of BM-MSCs-derived Exos towards inflammatory regions[24,44]; 3) active targeting, acquired from membrane proteins of Exos binding with biomarkers on the surface of tumor cells. Versatile expressed on/in human BM-MSCs derived Exos could be studied in ExoCarta data base[25]. For example, CD47, positive on Exos membrane, not only induces the "don't eat me" signal to avoid engulfing by monocytes in circulation, but also actively binds with phosphatidylserine on the surface of tumor cells[45]; 4) properties of tumor-homing inherited from BM-MSCs also contribute to the targeting capability. In addition, preferable biocompatibility benefited by hypoallergenic of BM-MSCs and natural homing ability without modification could enable Exos advantageous on delivery of nanomedicine.

3.6. *Drugs loading and anti-tumor efficacy in vitro*

Reversible electroporation was employed to load GEMP, and a sonication method was utilized to load PTX. After the removal of unbound drugs, the loading dose was analyzed and calculated by high performance liquid chromatography (HPLC). Approximate 1.5×10^9 Exos in 500 μL PBS 7.4, it contained 143.85 μg/mL

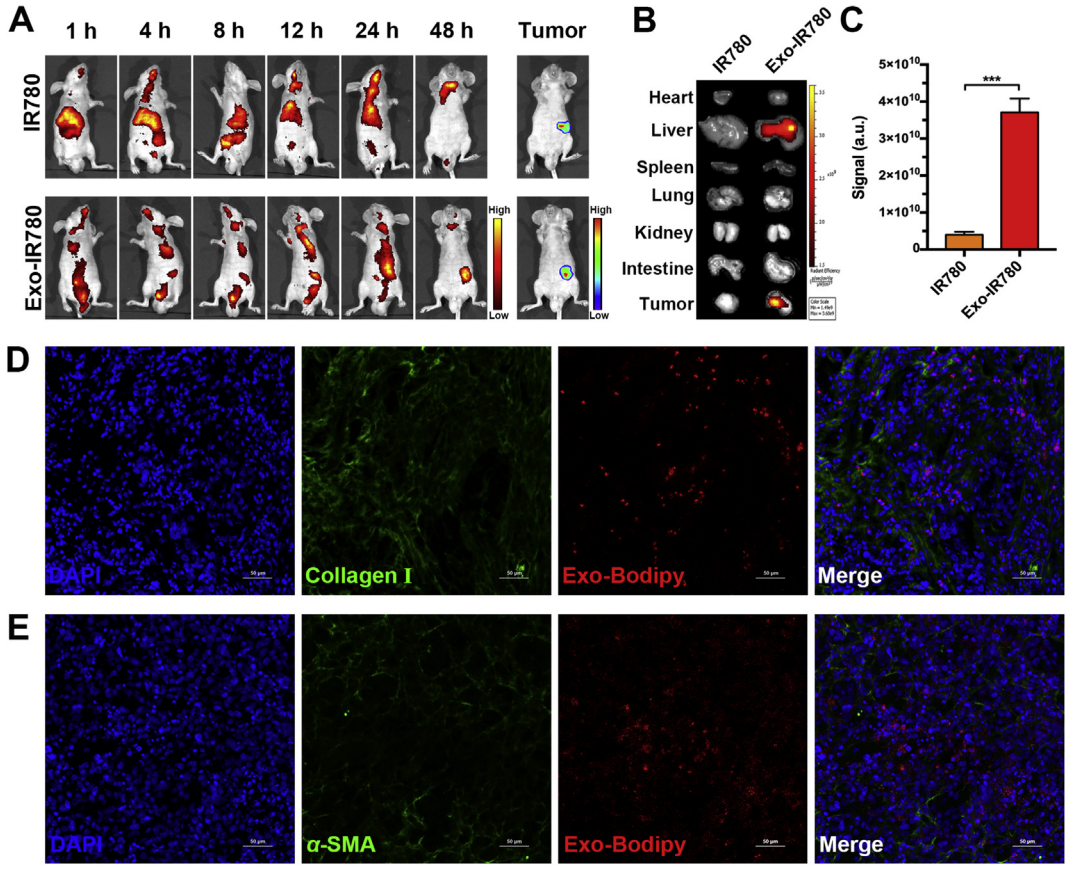

Figure 3 Accumulation and penetration in PDAC orthotopic model. (A) General fluorescent images at predesignated time point after intravenous injection of nomadic bodipy and Exo-Bodipy, rightmost represents tumor bioluminescence at 48 h. (B) Biodistribution of bodipy in major organs and whole tumors. (C) Fluorescence intensity of IR780 in different tumors, $^{***}P < 0.01$. (D) and (E) Tumor tissue immunofluorescent images under laser confocal scanning microscope. Blue: DAPI stained nuclei; green: AF488 labeled collagen I and α-SMA; red: bodipy labeled Exos. Scale bar: 50 μm, amplified 200×.

GEMP and 22.50 μg/mL PTX (Supporting Information Figs. S3A and B), and the concentration of GEM is 109.94 μg/mL (Fig. S3C). Zeta potentials of Exos, Exo-GEM and Exo-GEMP-PTX were −9.93 ± 0.46 V, −10.27 ± 0.62 and −10.46 ± 0.55 mV, respectively. The GEM encapsulation efficiency and loading capacity were 3.92% and 6.08%. The GEMP encapsulation efficiency and loading capacity were measured to be 5.92% and 8.78%, respectively. The PTX encapsulation efficiency and loading capacity were determined to be 2.62% and 1.25%. Meanwhile, the morphology of Exo-GEMP-PTX was observed under TEM (Supporting Information Fig. S4).

To evaluate the *in vitro* anti-tumor efficacy, MTT cytotoxicity assay, cellular apoptosis and cycle inhibition procedure were performed on MiaPaca-2 cells, respectively. Following incubated cells with different formulations, prominent proliferative inhibition was observed (Fig. 4A), except in the Exos group, which could fertilize the proliferation of cells. As to the standard chemotherapy regime, GEM plus nab-PTX (GEM+nab-PTX) was set as positive control, which showed less sensitive to MiaPaca-2 cells compared with Exo-loading GEMP and PTX (Exo-GEMP-PTX). After incubating cells with formulations for 15 h in concentration of 1 μmol/L (calculated in terms of GEM and GEMP, GEM:nab-PTX = 9:1), flowcytometry confirmed that Exo-GEMP-PTX induced significant higher ratio of cellular apoptosis (39.81 ± 1.42%), compared to Exos (1.10 ± 0.44%), GEM (10.96 ± 1.30%), Exos loading GEM (Exo-GEM, 16.00 ± 1.96%) and GEM+nab-PTX (33.02 ± 1.22%, $^{***}P < 0.01$, Fig. 4B and C). Tendency in cycle inhibition also similarly illustrated Exo-GEMP-PTX owned significant cytotoxic efficacy against MiaPaca-2 cell lines (Fig. 4D).

Down-regulation of pivotal proteins including human equilibrative nucleotide transporter 1 (hENT1) and deoxycytidine kinase (dCK), leads to decrease of GEM transported into cytoplasm and inefficient transformation into dFdCMP (GEMP), resulting in GEM-related chemoresistance[46]. Considering the significant difference between GEM and Exo-GEM groups (Fig. 4B−D), mutation of hENT1 may account for such phenomenon, because of different manners in transportation of GEM and Exo. To further elucidate the merit of Exos platform in overcoming chemoresistance, GEMP contained in cellular plasm within 8 h were measured. Standardized by 100 μg proteins, it was calculated that there had 18.77 ± 1.13 μg in Exo-GEMP-PTX group, 9.42 ± 0.399 μg in GEM+nab-PTX group, 11.46 ± 1.29 μg in Exo-GEM group, and 8.356 ± 0.382 μg in GEM group (Supporting Information Fig. S5). Higher endo-cellular dose of GEMP may indicate that GEMP delivered by Exos demonstrated advantageous on surmounting obstacles of chemoresistance.

3.7. *In vivo anti-tumor efficacy*

For the evaluation of anti-tumor efficacy *in vivo*, orthotopic PDAC models were prepared by implantation of luciferase stable transfected MiaPaca-2 cell lines into nude mice. As sketched in Fig. 5A, different formulations were intravenously injected (i.v.) every 3 days, and the body weight of mice was recorded every 3 days until the 27th day. All tumor-bearing animals in the treated

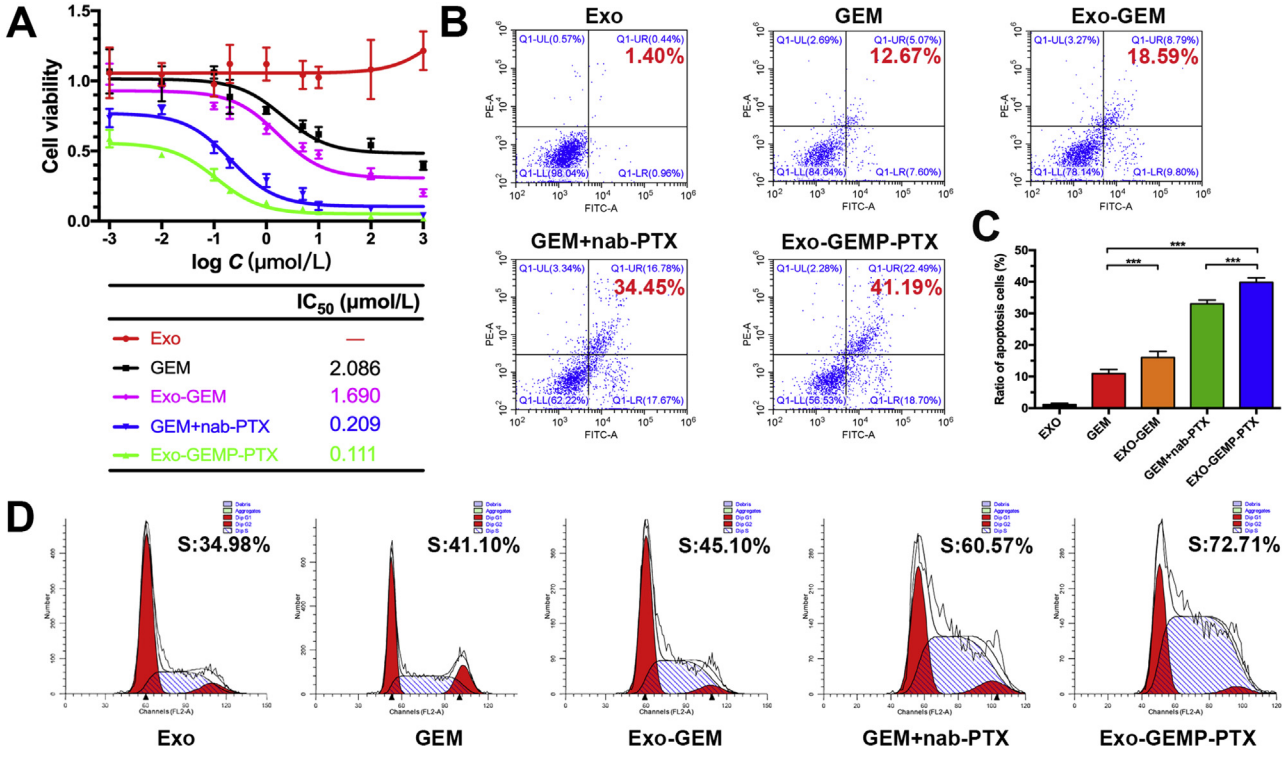

Figure 4 Anti-tumor efficacy *in vitro*. (A) IC_{50} and proliferative inhibition of Exos, GEM, Exo-GEM, GEM+nab-PTX and Exo-GEMP-PTX. (B) and (C) Cellular apoptosis induced by Exos, GEM, Exo-GEM, GEM+nab-PTX and Exo-GEMP-PTX, investigated by PI/Annexin-V stained flowcytometry, $^{***}P < 0.01$. (D) Ratio of cycle inhibition induced by Exo, GEM, Exo-GEM, GEM+nab-PTX and Exo-GEMP-PTX.

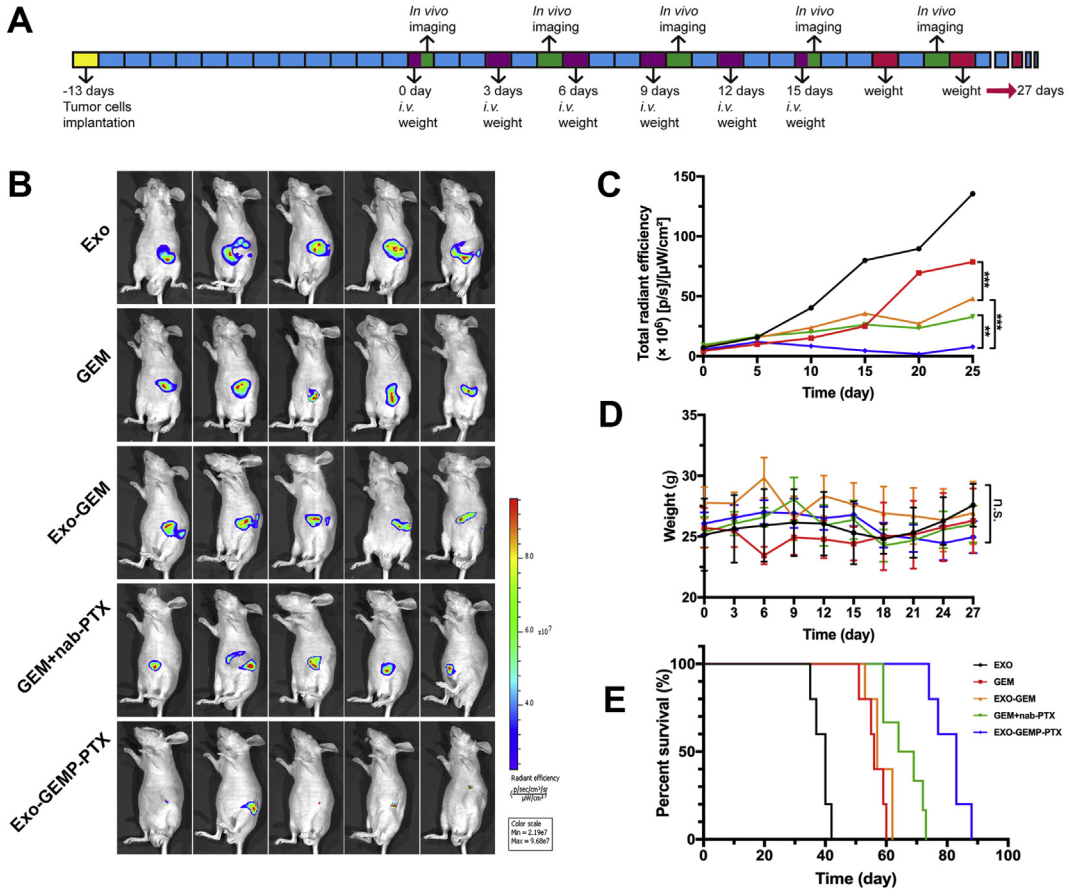

Figure 5 Anti-tumor efficacy *in vivo*. (A) Schematic orders of manipulations, including tumor implantation, intravenous injection of different formulations, weight, imaging *in vivo*. (B) Bioluminescence imaging *in vivo* on the 25th day. (C) Volume of tumors on the 0, 5, 10, 15, 20 and 25th day, $^{**}P < 0.05$, $^{***}P < 0.01$. (D) Body weight of tumor-bearing mice, n.s. represents no significance. (E) Survival curves.

groups maintained acceptable weight and changed insignificantly (Fig. 5B). Volume of tumors was monitored by *in vivo* imaging every 5 days, recorded as total radiant efficiency (Fig. 5C). After administration of 6 dose of 10 mg/kg GEM or GEMP in the corresponding groups, mice survival status was summarized in Fig. 5E, where apparently showed that Exo-GEMP-PTX group acquired the longest overall survival (88 days), compared with Exos group (42 days), GEM group (60 days), Exo-GEM group (63 days) and GEM+nab-PTX group (73 days). On the 25th day, bioluminescence imaging was performed to observe the volume of tumors (Fig. 5B), illustrating that Exo-GEMP-PTX could inhibit tumor growth to the greatest extent. The difference between GEM and Exo-GEM groups, demonstrated the Exos platform would benefit uptake of GEM, especially GEMP, which is regarded definite hardly uptake by cells.

On the 27th day, another three mice were sacrificed to evaluate the therapeutic efficacy in the view of pathology. H&E staining results showed there was no apparent changes occurred in major organs, demonstrating the systematic safety of all formulations (Supporting Information Fig. S6). Meanwhile, ECM stained by eosin declined in Exo-GEM group and GEM+nab-PTX group, especially in Exo-GEMP-PTX group (Supporting Information Fig. S7). Immunofluorescence staining of TUNEL (Fig. 6A and B) and Ki67 (Fig. 6C and D), elucidating that the superior therapeutic efficacy acquired by not only more apoptosis tumor cells, but also lower the proliferative activity.

Nab-PTX (Abraxane, Celgene; Summit, NJ, USA), a commercially available nano-medicine, was known as facilitating degradation of ECM and penetration of GEM[47]. To evaluate if the tumor mesenchymal component was affected by different treatment, the whole tumor tissue was imaged to further investigate the expression of collagen I and α-SMA. As shown in Fig. 6E and G, prominent decrease in the expression of α-SMA in Exo-GEMP-PTX group, could be listed as the evidence of great inhibited effect on tumor microenvironment. Meanwhile, Exo-GEMP-PTX group expressed decreased level of collagen I (Fig. 6F and H), especially in the marginal regions. Combining with previous assay of penetration in 3D spheroids and significant difference of therapeutic efficacy *in vivo*, we could conclude that Exo-GEMP-PTX show obvious advantages on the deep penetration, furthermore, on overcoming the limitation of chemoresistance.

4. Conclusions

In summary, we proved BM-MSCs derived Exos can home to pancreatic cancer efficiently and structure a co-delivery platform of GEMP and PTX. Benefiting from deformation and tetraspanin proteins, the Exos platform showed preferable penetration *in vivo*

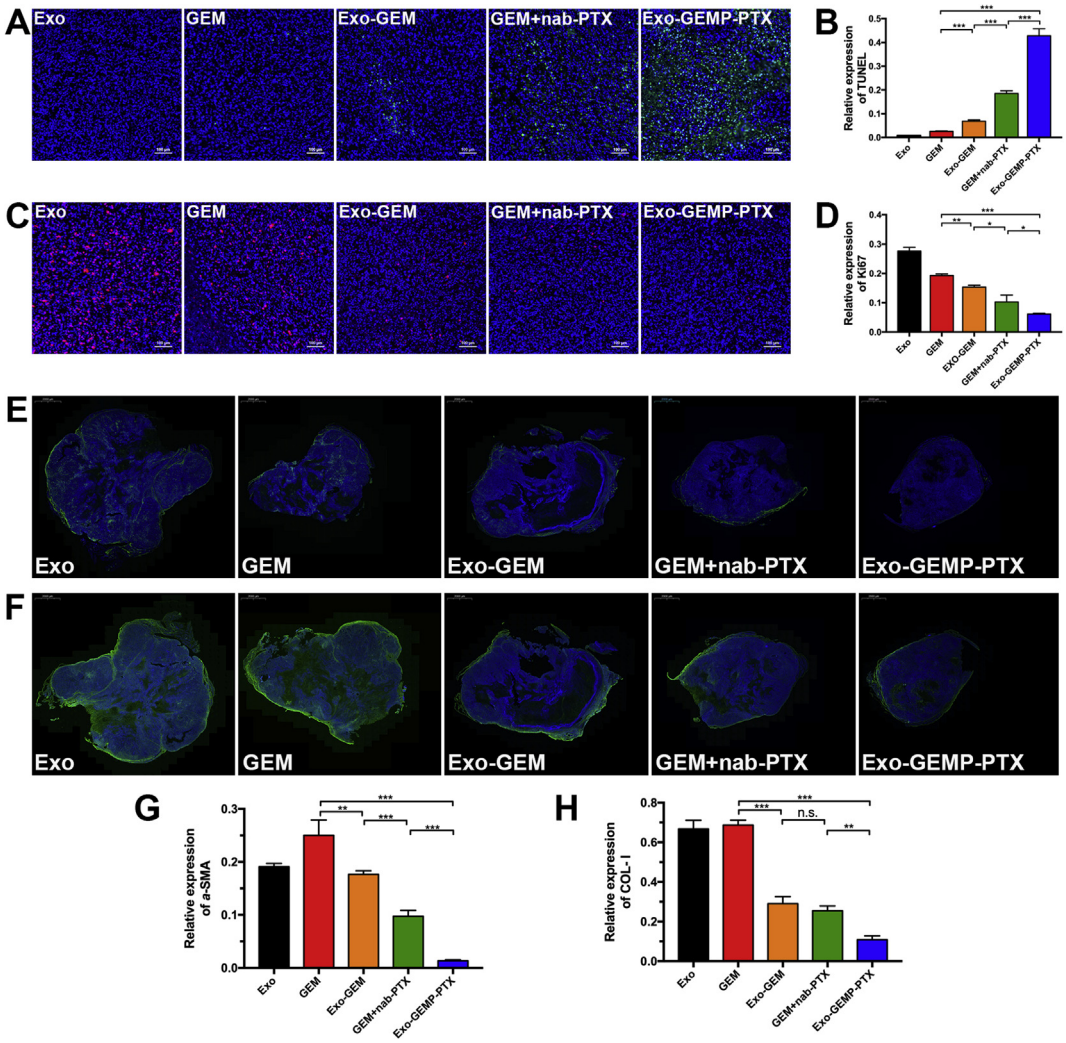

Figure 6 Hispathologic investigation of tumors in different treated groups. (A) and (B) TUNEL staining for the investigating of tumors apoptosis, and semi-quantitative analysis, scale bar 100 μm, $^{***}P < 0.01$. (C) and (D) Ki67 staining for the evaluation of proliferation activity of tumors after different treated, and semi-quantitative analysis, scale bar 100 μm, $^{*}P < 0.1$, $^{**}P < 0.05$, $^{***}P < 0.01$. Immunofluorescence staining of α-SMA (E) and collagen I (F), scanning of whole tumors, scale bar 2000 μm. Semi-quantitative analysis of α-SMA (G) and collagen I (H) in different groups, n.s. represents no significance, $^{**}P < 0.05$, $^{***}P < 0.01$.

and *in vitro*. Furthermore, loading GEMP and PTX acquired superior anti-tumor efficacy in GEM-related resistance PDAC both *in vitro* and *in vivo*. Based on the combined results, BM-MSCs derived Exos delivery system can overcome the tough obstacles in treatment of PDAC—chemoresistance and pathological barrier, which could serve well as a promising strategy of PDAC target therapy.

Acknowledgments

We wish to thank the kind help from Dr. Tao Sun, associate professor from Department of Pharmaceutics, School of Pharmacy, Fudan University (Shanghai, China), in synthesis of GEMP. We also acknowledge the support from National Science Fund for Distinguished Young Scholars (grant No. 81425023, China), National Natural Science Foundation of China (grant No. 81872808) and Program of Shanghai Academic Research Leader (18XD1400500, China).

Author contributions

Prof. Chen Jiang, Prof. Xiaoyi Ding and Yu Zhou conceived and designed the study. Yu Zhou performed all the experiments and wrote the paper. Prof. Chen Jiang and Prof. Xiaoyi Ding reviewed and edited the manuscript. Wenxi Zhou and Xinli Chen participated in isolation of exosomes, tracing exosomes and anti-tumor efficacy evaluation *in vivo*. Qingbing Wang participated in cell culture and preparation of PDAC orthotopic models. Chao Li and Qinjun Chen participated in the experiments of flow cytometry and immunofluorescence. Yu Zhang and Yifei Lu participated in preparation of tumor spheroids and data processing. All authors read and approved the manuscript.

Conflicts of interest

The authors have no conflicts of interest to declare.

Appendix A. Supporting information

Supporting data to this article can be found online at https://doi.org/10.1016/j.apsb.2019.11.013.

References

1. Siegel RL, Miller KD, Jemal A. Cancer statistics, 2017. *CA Cancer J Clin* 2017;**67**:7–30.
2. Gluth A, Werner J, Hartwig W. Surgical resection strategies for locally advanced pancreatic cancer. *Langenbeck's Arch Surg* 2015;**400**:757–66.
3. Werner J, Combs SE, Springfeld C, Hartwig W, Hackert T, Buchler MW. Advanced-stage pancreatic cancer: therapy options. *Nat Rev Clin Oncol* 2013;**10**:323–33.
4. Lunardi S, Muschel RJ, Brunner TB. The stromal compartments in pancreatic cancer: are there any therapeutic targets?. *Cancer Lett* 2014;**343**:147–55.
5. Samulitis BK, Pond KW, Pond E, Cress AE, Patel H, Wisner L, et al. Gemcitabine resistant pancreatic cancer cell lines acquire an invasive phenotype with collateral hypersensitivity to histone deacetylase inhibitors. *Cancer Biol Ther* 2015;**16**:43–51.
6. Li C, Wang J, Wang Y, Gao H, Wei G, Huang Y, et al. Recent progress in drug delivery. *Acta Pharm Sin B* 2019;**6**:1145–62.
7. Adiseshaiah PP, Crist RM, Hook SS, McNeil SE. Nanomedicine strategies to overcome the pathophysiological barriers of pancreatic cancer. *Nat Rev Clin Oncol* 2016;**13**:750–65.
8. Wong KM, Horton KJ, Coveler AL, Hingorani SR, Harris WP. Targeting the tumor stroma: the biology and clinical development of pegylated recombinant human hyaluronidase (PEGPH20). *Curr Oncol Rep* 2017;**19**:47.
9. Olive KP, Jacobetz MA, Davidson CJ, Gopinathan A, McIntyre D, Honess D, et al. Inhibition of Hedgehog signaling enhances delivery of chemotherapy in a mouse model of pancreatic cancer. *Science* 2009;**324**:1457–61.
10. Ady JW, Heffner J, Klein E, Fong Y. Oncolytic viral therapy for pancreatic cancer: current research and future directions. *Oncolytic Virotherapy* 2014;**3**:35–46.
11. Liang C, Shi S, Meng Q, Liang D, Ji S, Zhang B, et al. Do anti-stroma therapies improve extrinsic resistance to increase the efficacy of gemcitabine in pancreatic cancer?. *Cell Mol Life Sci* 2018;**75**:1001–12.
12. Von Hoff DD, Ervin T, Arena FP, Chiorean EG, Infante J, Moore M, et al. Increased survival in pancreatic cancer with nab-paclitaxel plus gemcitabine. *N Engl J Med* 2013;**369**:1691–703.
13. Pickup MW, Mouw JK, Weaver VM. The extracellular matrix modulates the hallmarks of cancer. *EMBO Rep* 2014;**15**:1243–53.
14. Raposo G, Stoorvogel W. Extracellular vesicles: exosomes, microvesicles, and friends. *J Cell Biol* 2013;**200**:373–83.
15. Yanez-Mo M, Siljander PR, Andreu Z, Zavec AB, Borras FE, Buzas EI, et al. Biological properties of extracellular vesicles and their physiological functions. *J Extracell Vesicles* 2015;**4**:27066.
16. Kourembanas S. Exosomes: vehicles of intercellular signaling, biomarkers, and vectors of cell therapy. *Annu Rev Physiol* 2015;**77**:13–27.
17. Batrakova EV, Kim MS. Using exosomes, naturally-equipped nanocarriers, for drug delivery. *J Control Release* 2015;**219**:396–405.
18. Yeo RW, Lai RC, Zhang B, Tan SS, Yin Y, Teh BJ, et al. Mesenchymal stem cell: an efficient mass producer of exosomes for drug delivery. *Adv Drug Deliv Rev* 2013;**65**:336–41.
19. Alvarez-Erviti L, Seow Y, Yin H, Betts C, Lakhal S, Wood MJ. Delivery of siRNA to the mouse brain by systemic injection of targeted exosomes. *Nat Biotechnol* 2011;**29**:341–5.
20. Wang J, Li W, Zhang L, Ban L, Chen P, Du W, et al. Chemically edited exosomes with dual ligand purified by microfluidic device for active targeted drug delivery to tumor cells. *ACS Appl Mater Interfaces* 2017;**9**:27441–52.
21. Tian Y, Li S, Song J, Ji T, Zhu M, Anderson GJ, et al. A doxorubicin delivery platform using engineered natural membrane vesicle exosomes for targeted tumor therapy. *Biomaterials* 2014;**35**:2383–90.
22. Ha D, Yang N, Nadithe V. Exosomes as therapeutic drug carriers and delivery vehicles across biological membranes: current perspectives and future challenges. *Acta Pharm Sin B* 2016;**6**:287–96.
23. Kabashima-Niibe A, Higuchi H, Takaishi H, Masugi Y, Matsuzaki Y, Mabuchi Y, et al. Mesenchymal stem cells regulate epithelial-mesenchymal transition and tumor progression of pancreatic cancer cells. *Cancer Sci* 2013;**104**:157–64.
24. Blogowski W, Bodnarczuk T, Starzynska T. Concise review: pancreatic cancer and bone marrow-derived stem cells. *Stem Cells Transl Med* 2016;**5**:938–45.
25. Mathivanan Suresh. *Exosome protein, RNA and lipid database*. Available from: http://www.exocarta.org; 2019.
26. Kamerkar S, LeBleu VS, Sugimoto H, Yang S, Ruivo CF, Melo SA, et al. Exosomes facilitate therapeutic targeting of oncogenic KRAS in pancreatic cancer. *Nature* 2017;**546**:498–503.
27. Hemler ME. Tetraspanin proteins mediate cellular penetration, invasion, and fusion events and define a novel type of membrane microdomain. *Annu Rev Cell Dev Biol* 2003;**19**:397–422.
28. Clergeot PH, Gourgues M, Cots J, Laurans F, Latorse MP, Pepin R, et al. PLS1, a gene encoding a tetraspanin-like protein, is required for penetration of rice leaf by the fungal pathogen *Magnaporthe grisea*. *Proc Natl Acad Sci U S A* 2001;**98**:6963–8.
29. Birhanu G, Javar HA, Seyedjafari E, Zandi-Karimi A. Nanotechnology for delivery of gemcitabine to treat pancreatic cancer. *Biomed Pharmacother* 2017;**88**:635–43.
30. Yang F, Jin C, Jiang Y, Li J, Di Y, Ni Q, et al. Liposome based delivery systems in pancreatic cancer treatment: from bench to bedside. *Cancer Treat Rev* 2011;**37**:633–42.
31. Poon C, He C, Liu D, Lu K, Lin W. Self-assembled nanoscale coordination polymers carrying oxaliplatin and gemcitabine for synergistic combination therapy of pancreatic cancer. *J Control Release* 2015;**201**:90–9.
32. El-Andaloussi S, Lee Y, Lakhal-Littleton S, Li J, Seow Y, Gardiner C, et al. Exosome-mediated delivery of siRNA *in vitro* and *in vivo*. *Nat Protoc* 2012;**7**:2112–26.
33. Kim MS, Haney MJ, Zhao Y, Mahajan V, Deygen I, Klyachko NL, et al. Development of exosome-encapsulated paclitaxel to overcome MDR in cancer cells. *Nanomedicine* 2016;**12**:655–64.
34. Van der Pol E, Boing AN, Harrison P, Sturk A, Nieuwland R. Classification, functions, and clinical relevance of extracellular vesicles. *Pharmacol Rev* 2012;**64**:676–705.
35. Rana S, Yue S, Stadel D, Zoller M. Toward tailored exosomes: the exosomal tetraspanin web contributes to target cell selection. *Int J Biochem Cell Biol* 2012;**44**:1574–84.
36. Colombo M, Raposo G, Thery C. Biogenesis, secretion, and intercellular interactions of exosomes and other extracellular vesicles. *Annu Rev Cell Dev Biol* 2014;**30**:255–89.
37. Kamisawa T, Wood LD, Itoi T, Takaori K. Pancreatic cancer. *Lancet* 2016;**388**:73–85.
38. Benien P, Swami A. 3D tumor models: history, advances and future perspectives. *Future Oncol* 2014;**10**:1311–27.

39. Simpson RJ, Kalra H, Mathivanan S. ExoCarta as a resource for exosomal research. *J Extracell Vesicles* 2012;**1**.
40. Charrin S, le Naour F, Silvie O, Milhiet PE, Boucheix C, Rubinstein E. Lateral organization of membrane proteins: tetraspanins spin their web. *Biochem J* 2009;**420**:133−54.
41. Hemler ME. Targeting of tetraspanin proteins—potential benefits and strategies. *Nat Rev Drug Discov* 2008;**7**:747−58.
42. Wrigley JD, Ahmed T, Nevett CL, Findlay JB. Peripherin/rds influences membrane vesicle morphology. Implications for retinopathies. *J Biol Chem* 2000;**275**:13191−4.
43. Tanaka HY, Kano MR. Stromal barriers to nanomedicine penetration in the pancreatic tumor microenvironment. *Cancer Sci* 2018;**109**:2085−92.
44. Harting MT, Srivastava AK, Zhaorigetu S, Bair H, Prabhakara KS, Toledano Furman NE, et al. Inflammation-stimulated mesenchymal stromal cell-derived extracellular vesicles attenuate inflammation. *Stem Cells* 2018;**36**:79−90.
45. Sharma B, Kanwar SS. Phosphatidylserine: a cancer cell targeting biomarker. *Semin Cancer Biol* 2018;**52**:17−25.
46. de Sousa Cavalcante L, Monteiro G. Gemcitabine: metabolism and molecular mechanisms of action, sensitivity and chemoresistance in pancreatic cancer. *Eur J Pharmacol* 2014;**741**:8−16.
47. Alvarez R, Musteanu M, Garcia-Garcia E, Lopez-Casas PP, Megias D, Guerra C, et al. Stromal disrupting effects of nab-paclitaxel in pancreatic cancer. *Br J Canc* 2013;**109**:926−33.